# ATLAS NOTE

ATLAS-CONF-2011-109

July 22, 2011


# Search for a heavy neutral particle decaying into an electron and a muon pair using $L = 0.87$ fb$^{-1}$ of ATLAS data

The ATLAS Collaboration



**Abstract**

A search for a high mass neutral particle that decays directly to the $e^{\pm}\mu^{\mp}$ final state is presented. The data sample was recorded by the ATLAS detector in $\sqrt{s} = 7$ TeV $pp$ collisions at the LHC from March to June 2011 and corresponds to an integrated luminosity of 0.87 fb$^{-1}$. The data are found to be consistent with the Standard Model background estimation. The high $e^{\pm}\mu^{\mp}$ mass region is used to set 95% confidence level upper limits on the production of two possible new physics processes: tau sneutrinos in an $R$-parity violating supersymmetric model and $Z'$-like vector bosons in a lepton flavor violating model.

Short-lived particles that decay into two oppositely signed leptons of different flavors, $e^{\pm}\mu^{\mp}$ ($e\mu$), $e^{\pm}\tau^{\mp}$ ($e\tau$), or $\mu^{\pm}\tau^{\mp}$ ($\mu\tau$), are predicted by a number of extensions to the Standard Model (SM). Examples include sneutrinos in $R$-parity violating (RPV) Supersymmetric (SUSY) models [1], and extra gauge $Z'$ bosons with lepton flavor violating (LFV) interactions [2]. This note reports a search for an excess of high invariant mass $e\mu$ ($m_{e\mu}$) events over SM predictions in $pp$ collisions at $\sqrt{s} = 7$ TeV at the LHC. The $e\mu$ final state is chosen due to its clean detector signature and low SM background in the high $m_{e\mu}$ region. Similar searches with the $e\mu$ final state have been reported previously by the CDF, D0 and ATLAS Collaborations [3, 4, 5, 6, 7, 8]. In this note, we report an updated search with a data sample approximately 25 times larger than that used for the previous ATLAS search [8] with improved sensitivity to new physics.

The ATLAS detector [9] is a multi-purpose particle physics apparatus with a forward-backward symmetric cylindrical geometry and near $4\pi$ coverage in solid angle [1]. The inner tracking detector (ID) consists of a silicon pixel detector, a silicon microstrip detector, and a transition radiation tracker. The ID is surrounded by a thin superconducting solenoid providing a 2 T magnetic field and by a finely-segmented, hermetic calorimeter system, which provides three-dimensional reconstruction of particle showers up to $|\eta| < 4.9$. Fine-granularity lead liquid-argon (LAr) electromagnetic calorimeters provide coverage for $|\eta| < 3.2$ to precisely measure the energy and position of electrons. The hadron calorimeter is based on iron-scintillating tiles sampling in the central region and on LAr sampling with copper or tungsten absorbers for $|\eta| > 1.7$. The muon spectrometer (MS) surrounds the calorimeters and consists of three large superconducting toroids, a system of precision tracking chambers and detectors for triggering.

The data sample used in this analysis was collected using single lepton ($e$ or $\mu$) triggers from March to June 2011. The total integrated luminosity is $865 \pm 39$ pb$^{-1}$. The preliminary luminosity uncertainty 4.5% is based on the 2010 luminosity calibration [10] which was transferred to the 2011 data by using the LAr forward calorimeter and the tile calorimeter current measurements. The trigger efficiency is measured to be 100%, with a precision of 1%, for $e\mu$ candidates that can pass the default selection criteria described below.

To select $e\mu$ candidates, the electron candidate is required to have $p_{\mathrm{T}} > 25$ GeV and to lie inside the pseudorapidity $|\eta| < 1.37$ or $1.52 < |\eta| < 2.47$. It is further required to pass the "medium" [11] quality definition, which is based on the calorimeter shower shape, track quality, and track matching with the calorimeter cluster. In addition, the electron is required to be isolated in the calorimeter with $E_{\mathrm{T}}^{\Delta R<0.4} < 10$ GeV, where $E_{\mathrm{T}}^{\Delta R<0.4}$ is defined as the transverse energy deposited in the calorimeter within a cone of radius $\Delta R = \sqrt{\Delta\eta^2 + \Delta\phi^2} = 0.4$ around the electron cluster. Corrections have been applied to account for energy leakage from the electron and energy deposition inside the isolation cone due to additional $pp$ collisions. The muon candidate must be reconstructed in both the ID and the MS, and have $p_{\mathrm{T}} > 25$ GeV and $|\eta| < 2.4$. Furthermore, the muon is required to be isolated in the ID with $p_{\mathrm{T}}^{\Delta R<0.4} < 10$ GeV, where $p_{\mathrm{T}}^{\Delta R<0.4}$ is defined as the scalar sum of the $p_{\mathrm{T}}$ of tracks associated to the primary vertex, within a cone of radius $\Delta R = 0.4$ around the muon track. Only tracks with $p_{\mathrm{T}} > 1$ GeV are used. Furthermore, only electrons separated from muons by $\Delta R > 0.2$ are considered.

The $e\mu$ candidate events are required to have exactly one electron and one muon with opposite charge satisfying the above selection criteria. Furthermore, events have to contain at least one primary vertex reconstructed with at least three associated tracks with $p_{\mathrm{T}} > 500$ MeV.

The SM processes that can produce an $e\mu$ signature can be divided into two categories: processes such as $Z/\gamma^* \to \tau\tau$, $t\bar{t}$, single top, $WW$, $WZ$ and $ZZ$, which can produce electrons and muons in the final state, and processes, referred to as instrumental background in this note, such as $W/Z$+$\gamma$, $W/Z$+jets and

[1] ATLAS uses a right-handed coordinate system with its origin at the nominal interaction point (IP) in the centre of the detector and the $z$-axis along the beam pipe. The $x$-axis points from the IP to the centre of the LHC ring, and the $y$ axis points upward. Cylindrical coordinates $(R, \phi)$ are used in the transverse plane, $\phi$ being the azimuthal angle around the beam pipe. The pseudorapidity is defined in terms of the polar angle $\theta$ as $\eta = -\ln\tan(\theta/2)$.

QCD multijets where the photon or one or two jets are reconstructed as leptons.

The contributions from processes listed in the first category as well as photon-related backgrounds are estimated using Monte Carlo (MC) samples generated at $\sqrt{s} = 7$ TeV. The detector response simulation [12] is based on the GEANT4 program [13]. Lepton reconstruction and identification efficiencies, energy scales and resolutions in the MC are corrected to the corresponding values measured in the data in order to improve the modeling of the background. The MC predictions are normalized to the data sample based on the integrated luminosity and cross sections of various physics processes. Top production is generated with MC@NLO [14] for $t\bar{t}$ and $Wt$, the Drell-Yan process is generated with PYTHIA [15], and the diboson processes are generated with HERWIG [16]. Higher order corrections to the predicted cross sections using these generators have been applied [17, 18, 19]. The $W/Z + \gamma$ instrumental background comes from the $W(\rightarrow \mu\nu)\gamma$ and $Z(\rightarrow \mu\mu)\gamma$ processes, where the photon is reconstructed as an electron. This background is estimated using events generated with MADGRAPH [20]. The $t\bar{t}$, $Wt$, $W/Z + \gamma$, $WW$, $WZ$ and $ZZ$ cross sections are assigned uncertainties of 12%, 12%, 10%, 5%, 7%, and 5% respectively. The integrated luminosity uncertainty and other smaller systematic uncertainties from the lepton trigger, reconstruction and identification efficiencies, energy (momentum) scale and resolution have been added in quadrature and are included in the total uncertainty.

The remaining jet instrumental backgrounds arise from the $W/Z$+jets and QCD multijet processes, where leptons are present from $b$- and $c$-hadron decays or at least one jet is misidentified as a lepton. These backgrounds account for ~30% of the expected $e\mu$ data yield and are estimated from data using a $4 \times 4$ matrix background estimation method described below. A looser lepton quality selection (called loose lepton here) is defined for each lepton type in addition to the default quality selection (called tight lepton here). For loose muons, the isolation requirement is dropped. For loose electrons, the "loose" electron identification criteria as defined in Ref. [11] are used and the isolation requirement is also dropped. The tight and loose lepton selections are then used to classify events where both leptons pass the loose requirements into four categories, depending on whether both leptons subsequently pass the tight requirement ($N_{pp}$), only one lepton fails the tight requirement and the other lepton passes the tight requirement ($N_{pf}$ or $N_{fp}$), or both leptons fail the tight requirement ($N_{ff}$). The sample composition can be estimated by solving a linear system of equations: $(N_{pp}, N_{pf}, N_{fp}, N_{ff})^T = \epsilon(N_{e\mu}, N_{ej}, N_{j\mu}, N_{jj})^T$, where $N_{e\mu}$ (or $N_{jj}$) is the number of events with two prompt leptons (or two non-prompt leptons), while $N_{ej}$ and $N_{j\mu}$ are the numbers of events with one prompt lepton and one non-prompt lepton. The matrix $\epsilon$ contains the probabilities for a loose quality lepton to pass the tight quality selection for both prompt and non-prompt leptons. The probability for prompt leptons is estimated by applying the loose and tight selections on $Z/\gamma^* \rightarrow \ell\ell(\ell = e, \mu)$ events. The probability for non-prompt leptons is estimated by applying the loose and tight selections on a sample of QCD dijet events. The matrix method is applied event by event and the overall jet instrumental background is found to be $984 \pm 29$ (stat) events. The breakdown of these contributions is estimated to be $N_{ej} = 330 \pm 28$ (stat), $N_{j\mu} = 70 \pm 12$ (stat) and $N_{jj} = 583 \pm 7$ (stat). The overall systematic uncertainty of 10.5% comes mainly from the uncertainty on the probability for a loose quality non-prompt muon to pass the tight quality selection.

Table 1 shows the number of events selected in data and the estimated background contributions with their uncertainties (both statistical and systematic uncertainties are included). A total of 3338 $e\mu$ candidates are observed, while the expectation from SM processes is $3408 \pm 230$ events. The $m_{e\mu}$ distribution is presented in Fig. 1 for data and background contributions. The distribution of observed events is compared to the expected background using a Kolmogorov-Smirnov test with statistical uncertainties only [21]. The test probability is 11%, consistent with the absence of a new physics signal. Table 2 shows the numbers of observed and predicted background events in eleven high $e\mu$ mass regions. Good agreement is found for all mass regions and no statistically significant data excess is observed. Limits are set on the contributions of new physics processes to the high mass region from two scenarios: the production of $\tilde{\nu}_\tau$ in an RPV SUSY model and of an LFV $Z'$ in extra-gauge boson models.

Table 1: Estimated backgrounds in the selected sample, together with the observed event yield. The total integrated luminosity is 0.87 $\text{fb}^{-1}$.

| Process | Number of events |
|---|---|
| $Z/\gamma^* \to \tau\tau$ | 614 ± 53 |
| $t\bar{t}$ | 1281 ± 168 |
| $WW$ | 318 ± 24 |
| Single top | 125 ± 17 |
| $WZ$ | 18.2 ± 1.9 |
| $W/Z + \gamma$ | 67 ± 11 |
| Jet instrumental background | 984 ± 105 |
| Total background | 3408 ± 230 |
| Data | 3338 |

Table 2: Estimated total backgrounds in the selected sample, together with the observed event yields for 11 high $e\mu$ mass regions.

| $m_{e\mu}$ | Data | SM prediction |
|---|---|---|
| > 200 GeV | 224 | 236 ± 21 |
| > 250 GeV | 119 | 111 ± 11 |
| > 300 GeV | 51 | 55 ± 6 |
| > 350 GeV | 29 | 30 ± 4 |
| > 400 GeV | 18 | 14.2 ± 2.2 |
| > 450 GeV | 9 | 8.2 ± 1.5 |
| > 500 GeV | 7 | 5.3 ± 1.1 |
| > 550 GeV | 3 | 3.4 ± 0.8 |
| > 600 GeV | 3 | 2.2 ± 0.7 |
| > 650 GeV | 1 | 0.9 ± 0.4 |
| > 700 GeV | 0 | 0.8 ± 0.4 |

The process $d\bar{d} \to \tilde{\nu}_\tau \to e\mu$ in a SUSY RPV model is considered. The RPV sneutrino couplings allowed in the supersymmetric Lagrangian are $\frac{1}{2}\lambda_{ijk}\hat{L}_i\hat{L}_j\hat{E}_k + \lambda'_{ijk}\hat{L}_i\hat{Q}_j\hat{D}_k$, where $L$ and $Q$ are the lepton and quark $SU(2)$ doublet superfields, and $E$ and $D$ denote the singlet fields for charged leptons and down type quarks, respectively. The indices $i, j, k = 1, 2, 3$ refer to the fermion generation numbers. The coupling constants $\lambda$ satisfy $\lambda_{ijk} = -\lambda_{jik}$. Only the tau sneutrino is considered in this note since stringent limits already exist on the electron sneutrino and muon sneutrino [1]. By fixing all RPV couplings except $\lambda'_{311}$ ($\tilde{\nu}_\tau$ to $d\bar{d}$) and $\lambda_{312}$ ($\tilde{\nu}_\tau$ to $e\mu$) to zero, and assuming that $\tilde{\nu}_\tau$ is the lightest supersymmetric particle, the contributions to the $e\mu$ final state originate from the $\tilde{\nu}_\tau$ only. The cross section is 0.154 pb for $m_{\tilde{\nu}_\tau} =$ 650 GeV, $\lambda'_{311} = 0.10$ and $\lambda_{312} = 0.05$ [22]. The total decay width is $\Gamma_{\tilde{\nu}_\tau} = (3\lambda'^2_{311}+2\lambda^2_{312})m_{\tilde{\nu}_\tau}/16\pi$. Using couplings that are consistent with the current limits, the decay width is less than 1 GeV for $m_{\tilde{\nu}_\tau} = 1$ TeV, which is well below the contribution from detector resolution. MC samples with $\tilde{\nu}_\tau$ masses ranging from 0.1 to 1 TeV are generated with HERWIG [16, 23].

An $e\mu$ resonance also appears in models containing a heavy neutral gauge boson, $Z'$ [24], with non-diagonal lepton flavor couplings. Interpretation of the results of rare muon decay searches has placed very stringent limits on the combination of the mass and the coupling to $ee$ and $e\mu$ in such models [2]. Using the data presented in this note, a limit on the production cross section times branching ratio to $e\mu$ can be placed on a $Z'$-like vector boson. To calculate the efficiency and acceptance, the $Z'$ is assumed to have the same quark and lepton couplings as the SM $Z$. The cross section is 0.61 pb for $m_{Z'} = 700$ GeV [25]. MC samples with $Z'$ masses ranging from 0.7 to 2 TeV are generated with PYTHIA.

Both $\tilde{\nu}_\tau$ and $Z'$ samples are processed through the standard chain of the ATLAS simulation and reconstruction. The overall product of acceptance and efficiency is 36% for $m_{\tilde{\nu}_\tau} = 100$ GeV and increases to 65% for $m_{\tilde{\nu}_\tau} = 1$ TeV. The corresponding number is 60% for $m_{Z'} = 700$ GeV and increases to 64% for $m_{Z'} > 1000$ GeV. The predicted $m_{e\mu}$ distributions for a $\tilde{\nu}_\tau$ with $m_{\tilde{\nu}_\tau} = 650$ GeV and a $Z'$ with $m_{Z'} = 700$ GeV are also shown in Fig. 1.

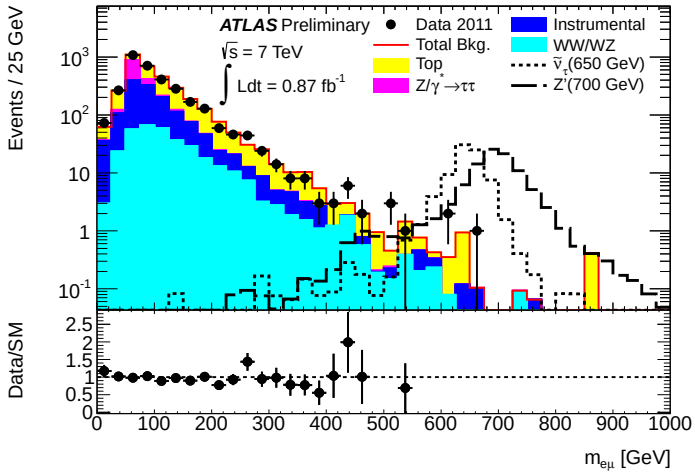


Figure 1: Observed and predicted $e\mu$ invariant mass distributions. Signal simulations are shown for $m_{\tilde{\nu}_\tau} = 650$ GeV and $m_{Z'} = 700$ GeV. The couplings $\lambda'_{311} = 0.10$ and $\lambda_{312} = 0.05$ are used for the RPV $\tilde{\nu}_\tau$ model. The production cross section is assumed to be the current published limit of 0.178 pb for the LFV $Z'$ model. The ratio plot at the bottom includes only statistical uncertainties.

The $m_{e\mu}$ spectrum is examined for the presence of a new heavy particle. For each assumed $m_{\tilde{\nu}_\tau}$ value, a search region, which depends on the simulated $e\mu$ mass resolution, is used. The numbers of observed and predicted background and signal events in each search range are used to set an upper limit on $\sigma(pp \to \tilde{\nu}_\tau)\times\mathrm{BR}(\tilde{\nu}_\tau \to e\mu)$. A Bayesian method [26] with a uniform prior for the signal cross section

as a function of $m_{\tilde{\nu}_\tau}$ is used. Fig. 2a shows the expected and observed 95% confidence level (C.L.) limits, as a function of $m_{\tilde{\nu}_\tau}$, together with the limits previously published by ATLAS [8], which were based on 35 pb$^{-1}$ of data, and the ±1 and ±2 standard deviation uncertainty bands. For a $\tilde{\nu}_\tau$ with a mass of 100 GeV (1 TeV), the limit on the cross section times branching ratio is 130 (11) fb. The theoretical cross sections for $\lambda'_{311} = 0.10$, $\lambda_{312} = 0.05$ and $\lambda'_{311} = 0.01$, $\lambda_{312} = 0.01$ are also shown. Tau sneutrinos with a mass below 0.44 TeV are excluded, assuming coupling values $\lambda'_{311} = 0.01$, $\lambda_{312} = 0.01$. The limits obtained extend 7 (14) times beyond the previous results. The 95% C.L. observed upper limits on $\lambda'_{311}$ as a function of $m_{\tilde{\nu}_\tau}$ are shown in Fig. 2b for three values of $\lambda_{312}$, together with the exclusion region obtained from the D0 experiment [7] and previously by the ATLAS experiment [8]. The limits are significantly better than the limits from the previous ATLAS analysis using 35pb$^{-1}$ of data.

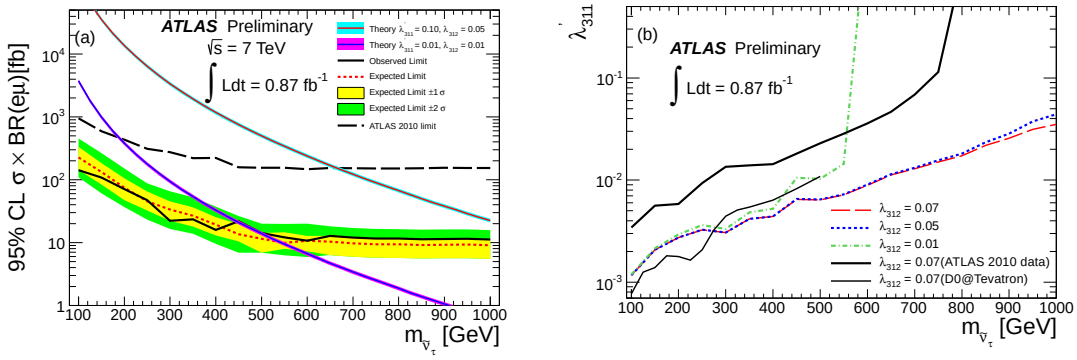


Figure 2: (a) The observed 95% C.L. upper limits on $\sigma(pp \to \tilde{\nu}_\tau) \times \mathrm{BR}(\tilde{\nu}_\tau \to e\mu)$ as a function of $m_{\tilde{\nu}_\tau}$. The expected limits are also shown together with the ±1 and ±2 standard deviation uncertainty bands. The previous ATLAS published limit and two theoretical cross sections for $\lambda'_{311} = 0.10$, $\lambda_{312} = 0.05$ and $\lambda'_{311} = 0.01$, $\lambda_{312} = 0.01$ are also shown. (b) The 95% C.L. upper limits on the $\lambda'_{311}$ coupling as a function of $m_{\tilde{\nu}_\tau}$ for three values of $\lambda_{312}$. The regions above the three curves represent ranges of $\lambda'_{311}$ values that are excluded. These results are compared with the exclusion regions obtained from the D0 experiment and the previously published ATLAS analysis.

A similar method is used to set limits on the LFV $Z'$-like vector boson, using only events with $m_{e\mu} > 550$ GeV; this cut was chosen to maximize sensitivity for the 0.7 TeV mass point. The 95% C.L. upper limits on $\sigma(pp \to Z') \times \mathrm{BR}(Z' \to e\mu)$ are shown in Fig. 3. The expected limit is the same as the observed limit because the median value of the SM expectation is 3.0, and the observation is also 3 events. For a $Z'$ with mass of 0.7 TeV (2.0 TeV), the limit on the cross section times branching ratio is 10.6 fb (10.0 fb). This result improves upon previous ATLAS limits by roughly a factor of 20.

In conclusion, a search has been performed for high mass $e\mu$ events using $pp$ collision data at $\sqrt{s} =$ 7 TeV recorded by the ATLAS detector. The observed $m_{e\mu}$ distribution is found to be consistent with SM predictions. With no evidence for new physics, 95% C.L. exclusion limits are placed on the production cross sections and RPV coupling values of the tau sneutrinos in an RPV SUSY model, which significantly improve the previous results. More stringent constraints are also set on the production cross sections of $Z'$ bosons in an LFV model. These two benchmark models can be used to represent the production of any narrow scalar and vector particles that can decay to the $e\mu$ final state.

## References


[1] R. Barbier *et al.*, Phys. Rep. **420**, 1 (2005).

[2] B. Murakami, Phys. Rev. D **65**, 055003 (2002).

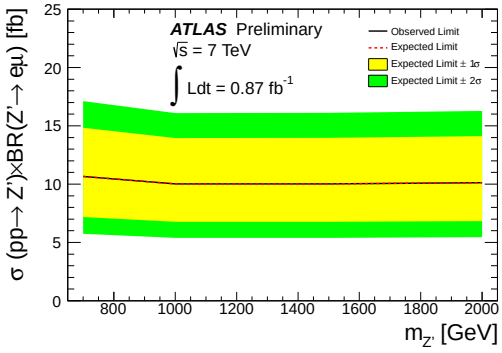


Figure 3: The observed 95% C.L. upper limits on $\sigma(pp \to Z') \times \mathrm{BR}(Z' \to e\mu)$. The expected limits are also shown together with the $\pm 1$ and $\pm 2$ standard deviation uncertainty bands. The observed and expected limits overlap as discussed in the text.


[3] CDF Collaboration, Phys. Rev. Lett. **91**, 171602 (2003).

[4] CDF Collaboration, Phys. Rev. Lett. **96**, 211802 (2006).

[5] CDF Collaboration, Phys. Rev. Lett. **105**, 191801 (2010).

[6] D0 Collaboration, Phys. Rev. Lett. **100**, 241803 (2008).

[7] D0 Collaboration, Phys. Rev. Lett. **105**, 191802 (2010).

[8] ATLAS Collaboration, Phys. Rev. Lett. **106**, 251801 (2011).

[9] ATLAS Collaboration, JINST **3**, (2008) S08003.

[10] ATLAS Collaboration, Updated Luminosity Determination in $pp$ Collisions at $\sqrt{s} = 7$ TeV using the ATLAS Detector, ATLAS-CONF-2011-011, Mar, 2011.

[11] ATLAS Collaboration, JHEP **1012** (2010) 060.

[12] ATLAS Collaboration, Eur. Phys. J. C **70**, (2010), 823.

[13] GEANT4 Collaboration, Nucl. Instrum. Meth. A **506** 250 (2003).

[14] S. Frixione and B.R. Webber, JHEP **0206** (2002) 029; S. Frixione, E. Laenen and P. Motylinski, JHEP **0603** (2006) 092; S. Frixione *et al.*, JHEP **0807** (2008) 029.

[15] T. Sjostrand, S. Mrenna, and P.Z. Skands, JHEP **0605** (2006) 026.

[16] G. Marchesini *et al.*, Computer Phys. Commun. 67 (1992) 465; G. Corcella *et al.*, JHEP **0101** (2001) 010.

[17] K. Melnikov and F. Petriello, Phys. Rev. D **74**, 114017 (2006).

[18] R. Bonciani *et al.*, Nucl. Phys. B **529**, 424 (1998).

[19] J. Campbell, R. Ellis and D. Rainwater, Phys. Rev. D **68**, 094021 (2003).

[20] J. Alwall *et al.*, JHEP **0709** (2007) 028.

[21] Kolmogorov, A., G. Inst. Ital. Attuari, 4, 83 (1933); Smirnov. N.V., Annals of Mathematical Statistic, 19, 279 (1948).

[22] S.M. Wang *et al.*, Phys. Rev. D **74**, 057902 (2006); S.M. Wang et al., Chin. Phys. Lett. **25**, 58 (2008).

[23] S. Moretti *et al.*, JHEP **0204** (2002) 028.

[24] P. Langacker, Rev. Mod. Phys. **81**, 1199 (2009).

[25] R. Hamberg, W.L. van Neerven, and T. Matsuura, Nucl. Phys. B **359**, 343 (1991).

[26] J. Heinrich and L. Lyons, Annual Review of Nuclear and Particle Science, **57** 145 (2007).

# 1 Auxilliary material

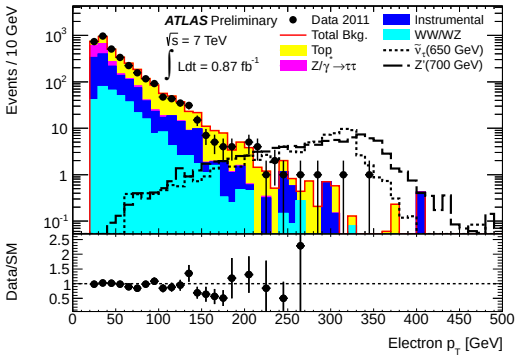


Figure 4: Observed and SM predicted electron $p_T$ distributions. The signal simulation is shown for $m_{\tilde{\nu}_\tau} = 650$ GeV and $m_{Z'} = 700$ GeV. The couplings $\lambda'_{311} = 0.10$ and $\lambda_{312} = 0.05$ are used for the RPV $\tilde{\nu}_\tau$ model. The production cross section is assumed to be the current published limit of 0.178 pb for the LFV $Z'$ model.

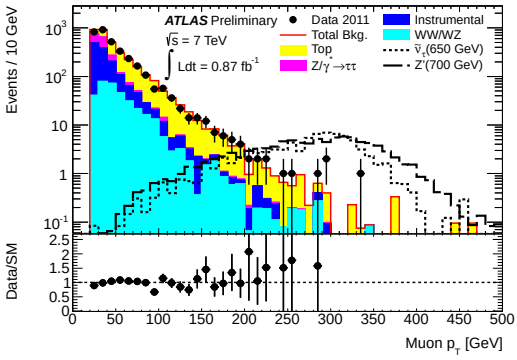


Figure 5: Observed and SM predicted muon $p_T$ distributions. The signal simulation is shown for $m_{\tilde{\nu}_\tau} = 650$ GeV and $m_{Z'} = 700$ GeV. The couplings $\lambda'_{311} = 0.10$ and $\lambda_{312} = 0.05$ are used for the RPV $\tilde{\nu}_\tau$ model. The production cross section is assumed to be the current published limit of 0.178 pb for the LFV $Z'$ model.

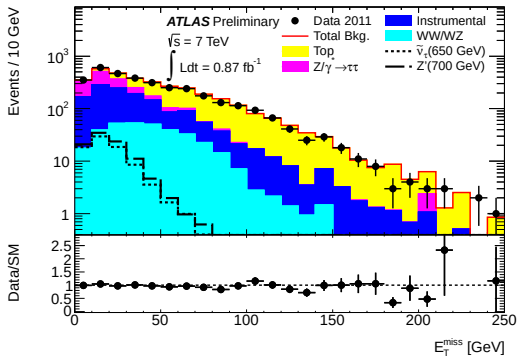


Figure 6: Observed and SM predicted $E_{\mathrm{T}}^{\mathrm{miss}}$ distributions. The signal simulation is shown for $m_{\tilde{\nu}_\tau} = 650\,\mathrm{GeV}$ and $m_{Z'} = 700\,\mathrm{GeV}$. The couplings $\lambda'_{311} = 0.10$ and $\lambda_{312} = 0.05$ are used for the RPV $\tilde{\nu}_\tau$ model. The production cross section is assumed to be the current published limit of 0.178 pb for the LFV $Z'$ model.

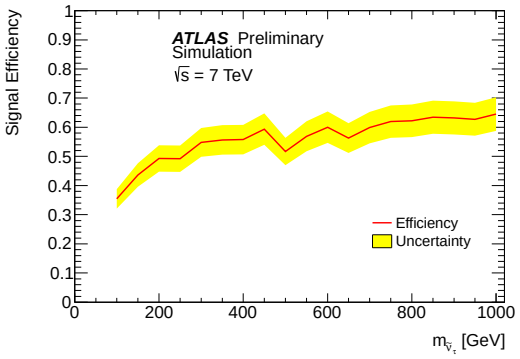


Figure 7: RPV sneutrino signal selection efficiency as a function of sneutrino mass.

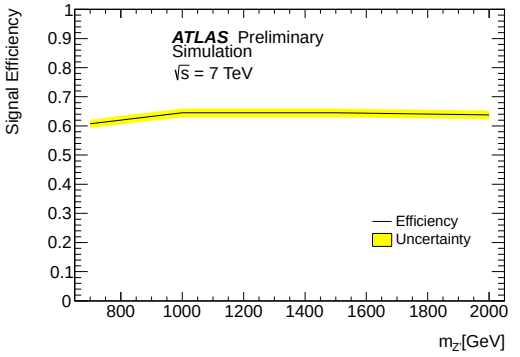


Figure 8: $Z'$ signal selection efficiency as a function of $Z'$ mass.

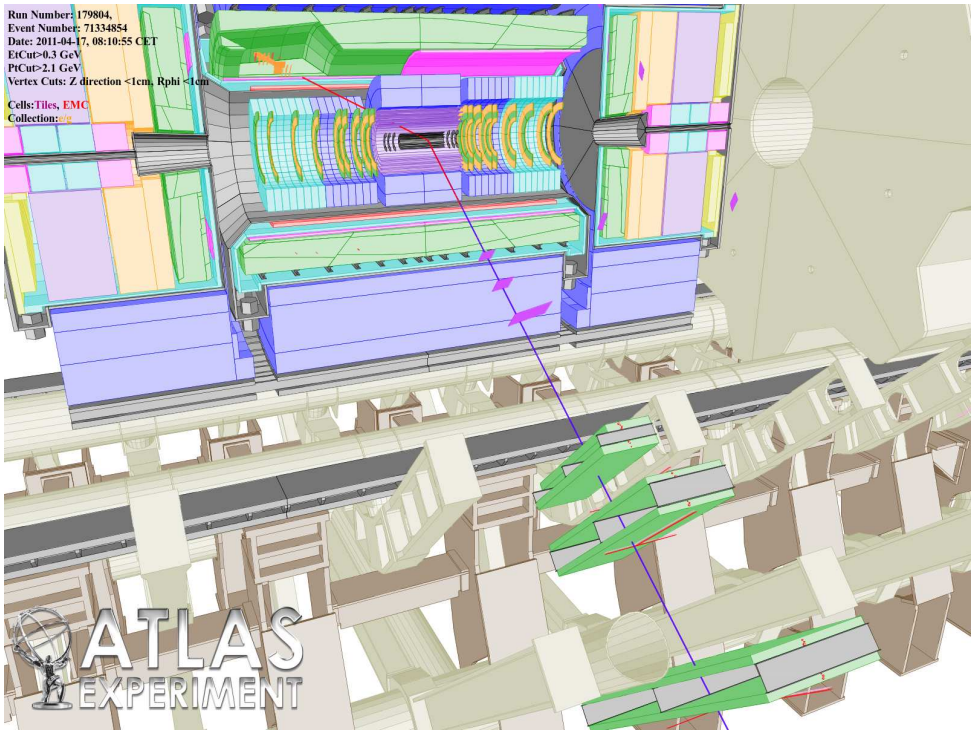


Figure 9: Event display for run 179804 event 71334854, the $e\mu$ pair in this event gives the highest $m_{e\mu}$. In this event, electron $p_{\mathrm{T}} = 341$ GeV, $\eta = -1.17$, $\phi = 0.91$; muon $p_{\mathrm{T}} = 216$ GeV, $\eta = 0.14$, $\phi = -2.36$; $m_{e\mu} = 662$ GeV, $\Delta\phi_{e\mu} = 3.02$ and $E_{\mathrm{T}}^{\mathrm{miss}} = 132$ GeV. There is no jet with $p_{\mathrm{T}} > 30$ GeV in this event.